

~~CONFIDENTIAL~~

NACA RM H55G26

UNCLASSIFIED

NACA

RESEARCH MEMORANDUM

FLIGHT MEASUREMENTS OF DIRECTIONAL STABILITY TO A MACH
NUMBER OF 1.48 FOR AN AIRPLANE TESTED WITH THREE
DIFFERENT VERTICAL TAIL CONFIGURATIONS

By Hubert M. Drake, Thomas W. Finch, and James R. Peele

High-Speed Flight Station
Edwards, Calif.

CLASSIFIED DOCUMENT

This material contains information affecting the National Defense of the United States within the meaning of the espionage laws, Title 18, U.S.C., Secs. 793 and 794, the transmission or revelation of which in any manner to an unauthorized person is prohibited by law.

NATIONAL ADVISORY COMMITTEE
FOR AERONAUTICS

WASHINGTON

October 7, 1955

CLASSIFICATION CHANGED

UNCLASSIFIED

To: *70800*
of R.A. 129 Effective Date 7/17/58
954

~~CONFIDENTIAL~~

NATIONAL ADVISORY COMMITTEE FOR AERONAUTICS

RESEARCH MEMORANDUM

FLIGHT MEASUREMENTS OF DIRECTIONAL STABILITY TO A MACH
NUMBER OF 1.48 FOR AN AIRPLANE TESTED WITH THREE
DIFFERENT VERTICAL TAIL CONFIGURATIONS

By Hubert M. Drake, Thomas W. Finch, and James R. Peele

SUMMARY

Flight tests have been performed to measure the directional stability of a fighter-type airplane over the Mach number range from 0.72 to 1.48. The tests were made at altitudes of 40,000 feet and 30,000 feet and employed three different vertical tails of varying aspect ratio or area, or both.

These tests showed that the directional stability for all tail configurations increased with an increase in tail aspect ratio or area, or both, over the entire Mach number range and decreased with increasing supersonic Mach number above 1.15.

INTRODUCTION

The decrease in directional stability with increasing supersonic Mach number during flight tests of research airplanes has been discussed previously in references 1 to 3. In general this decrease results from the fact that with increasing supersonic Mach number the lift-curve slope of the vertical tail decreases while the unstable directional moment of the fuselage remains essentially constant. If the directional stability of the airplane becomes sufficiently low, deterioration of the dynamic stability can result (refs. 1 to 3) and, if the directional stability becomes zero, an actual divergence can occur.

With the advent of fighter airplanes capable of appreciable supersonic Mach numbers, the problem of adequate directional stability at supersonic speed has become of immediate importance. A fighter airplane having a 45° swept wing and supersonic performance capabilities is being utilized for flight research by the NACA High-Speed Flight Station at Edwards, Calif. During rate-of-roll tests this fighter airplane exhibited violent cross-coupling behavior as reported in reference 4. Low

directional stability was considered to have contributed to the violence of the behavior. An investigation was undertaken, therefore, to determine in flight the directional stability of the airplane. During the investigation two additional vertical tail configurations with increased area and aspect ratio became available and were included in the tests.

This paper gives the results of the measurements of directional stability for these three tails within the Mach number range from 0.72 to about 1.48.

SYMBOLS

A	aspect ratio
b	wing span, ft
C_l	rolling-moment coefficient, $\frac{\text{Rolling moment}}{qSb}$
$C_{l\beta}$	airplane effective dihedral parameter, $\frac{\partial C_l}{\partial \beta}$, deg ⁻¹
C_{N_A}	airplane normal-force coefficient, $\frac{nW}{qS}$
C_n	yawing-moment coefficient, $\frac{\text{Yawing moment}}{qSb}$
$C_{n\beta}$	airplane directional stability parameter, $\frac{\partial C_n}{\partial \beta}$, deg ⁻¹
c	chord, ft
\bar{c}	mean aerodynamic chord, ft
g	acceleration due to gravity, ft/sec ²
h_p	altitude, ft
I_X	moment of inertia about X-axis, slug-ft ²
I_Y	moment of inertia about Y-axis, slug-ft ²
I_Z	moment of inertia about Z-axis, slug-ft ²

I_{YZ}	product of inertia, slug-ft ²
i_t	angle of tail incidence measured from line parallel to longitudinal axis of airplane, deg
M	Mach number
n	load factor, g units
P	period of lateral oscillation, sec
p	rolling angular velocity, radians/sec
q	dynamic pressure, lb/sq ft
q	pitching angular velocity, radians/sec
r	yawing angular velocity, radians/sec
S	wing area, ft ²
$T_{1/2}$	time to damp to half amplitude of lateral oscillation, sec
t	time, sec
W	weight, lb
α	indicated angle of attack, deg
β	indicated angle of sideslip, deg
δ_{at}	total aileron deflection, deg
δ_r	rudder deflection, deg
$\Lambda_{c/4}$	sweepback at 0.25 chord, deg
λ	taper ratio

AIRPLANE AND INSTRUMENTATION

The airplane utilized in this investigation is a fighter type with a single turbojet engine and a low swept wing and tail. A three-view drawing of the airplane with the original vertical tail is shown in

figure 1. Figure 2 presents a photograph of the airplane. The geometric and mass characteristics of the airplane are given in table 1.

The tests utilized three vertical tails characterized by differing areas and aspect ratios as follows:

	Area, sq ft	Aspect ratio
Tail A	33.5	1.13
Tail B	37.3	1.49
Tail C	42.7	1.49

Drawings of the three tails are shown in figure 3. Figure 4 presents a photograph of two airplanes showing tails A and C. The same rudder was used with all tails.

Complete stability and control instrumentation was installed for the flight research reported in this paper. The angle of attack, angle of sideslip, airspeed, and altitude were sensed on the nose boom. The Mach numbers presented are based on a preliminary calibration of the airspeed installation and are considered accurate to ± 0.02 at subsonic speeds and to ± 0.01 at supersonic speeds. The angle of attack and angle of sideslip are presented as measured.

TESTS AND DATA REDUCTION

Rudder pulses were performed to determine the period and damping of the lateral motions. The maneuvers were performed by abruptly deflecting the rudder pedals, returning them to neutral, then holding them fixed. The stick was held fixed throughout the maneuver. Representative maneuvers are presented in time history form in figure 5. Maneuvers were performed in level flight as shown in the following tabulation, except for the maneuvers at Mach numbers greater than 1.35 which were performed in dives at altitudes above 33,000 feet.

M	Altitude, ft	Vertical tail
0.72 to 0.74	30,000	A, B, and C
0.84 to 1.34	40,000	A
0.78 to 1.39	40,000	B
0.72 to 1.48	40,000	C

It was found that the simplified method of determining the value of the directional stability parameter $C_{n\beta}$ given in reference 5 was inadequate for this airplane. Therefore, the following expression was used (see appendix A for derivation):

$$C_{n\beta} = \left[\left(\frac{2\pi}{P} \right)^2 + \left(\frac{0.693}{T_{1/2}} \right)^2 \right] \frac{I_Z}{57.3qSb} - \frac{I_{XZ}}{I_X} C_{l\beta} + \alpha \frac{I_Z}{I_X} C_{l\beta}$$

It may be noted that this expression includes the single-degree-of-freedom relation of reference 5 modified to include the effects of damping, product of inertia, and an angle-of-attack term. The expression gives the value of $C_{n\beta}$ as measured about the body axis. The

product-of-inertia term is very small since the principal axis is estimated by the manufacturer to be inclined only about $1/2^\circ$ down at the nose for an average test weight. Unpublished wind-tunnel measurements of $C_{l\beta}$ for Mach numbers up to 1.0 were used in the equation. Since above $M = 1.0$ the angles of attack were generally less than 3° and $C_{l\beta}$ is quite small, the angle-of-attack term is considered small enough to be neglected at supersonic speeds.

RESULTS AND DISCUSSION

The time histories of maneuvers at $M = 0.74$ and at $M = 1.38$ in figure 5 were performed with tail B but are representative of all three tails. In most cases the pedals and stick were held fixed subsequent to the pulse; however, small control surface movements did occur.

Figure 6 shows the measured period and damping for the three tail configurations. These data are presented for an altitude of 40,000 feet with the exception of the points above $M = 1.35$ which, as mentioned previously, were obtained in dives between 40,000 feet and 33,000 feet. For any given tail there is very little scatter in the periods measured, indicating the small control movements did not unduly influence the period. The measured damping, however, shows considerable scatter. This condition reflects the difficulty of measuring the damping and possibly the effect of the small control motions. For the most part, the periods show a general decrease with an increase of Mach number at subsonic speeds and show an almost constant value at supersonic speeds. With each of the three tail configurations, the measured variation of damping of the airplane indicates a region of reduced stability (increased time to damp) at transonic speeds with less time required to damp to half amplitude at Mach numbers above and below this region.

The values of the directional stability parameter $C_{n\beta}$ were computed from the values of P and $T_{1/2}$ in figure 6. Figure 7 presents the Mach number variation of $C_{n\beta}$ determined for each of the tail configurations. The value of $C_{n\beta}$ increases with increasing tail size as would be expected from the increase in aspect ratio or area, or both.

The decrease in $C_{n\beta}$ anticipated with increasing supersonic Mach number (ref. 2) is quite pronounced particularly above $M \approx 1.15$. With tail C, for example, the airplane lost about half its directional stability between $M = 1.15$ and $M = 1.48$. A measure of the improvement in $C_{n\beta}$ (produced by increasing tail area and aspect ratio) is shown by the fact that a value of $C_{n\beta} = 0.001$ was reached at $M = 1.22$ with tail A, but with tail C the value of $C_{n\beta} = 0.001$ was not reached until about $M = 1.48$.

An unpublished value of $C_{n\beta} = 0.0019$ measured in the Langley 4- by 4-foot supersonic pressure tunnel at $M = 1.41$ is shown in figure 7. When this value is corrected for aeroelastic effects estimated by the manufacturer ($\Delta C_{n\beta} = -0.00052$) and the effect of turning the air flow at the intake duct ($\Delta C_{n\beta} = -0.00025$), a value of $C_{n\beta}$ nearly equivalent to that measured in flight is obtained.

The required value of $C_{n\beta}$ for reasonable handling qualities is, of course, not indicated in these tests but must be determined by the performance of other maneuvers such as the aileron rolls presented in reference 4. That $C_{n\beta}$ may become very small or neutral at high Mach numbers, however, indicates that under some conditions poor dynamic stability may be encountered, as for the Douglas D-558-II airplane (refs. 1 to 3), or an actual static directional divergence may occur.

CONCLUDING REMARKS

Flight tests of a fighter-type airplane with three different vertical tail configurations over the Mach number range from 0.72 to 1.48 indicate, as would be expected, that the directional stability increased with an increase in tail aspect ratio or area, or both, over the entire Mach number range and decreased with increasing supersonic Mach number for all tail configurations.

The Mach number at which a value of the directional stability parameter $C_{n\beta}$ had decreased to 0.001 was increased from a Mach number of 1.22 to a Mach number of 1.48 by increasing the tail area 27 percent and increasing the tail aspect ratio 32 percent.

High-Speed Flight Station,
National Advisory Committee for Aeronautics,
Edwards, Calif., July 20, 1955.

APPENDIX A

DERIVATION OF $C_{n\beta}$ EQUATION

The three lateral equations of motion containing terms pertinent to the derivation of $C_{n\beta}$ are written as

$$\dot{\beta} = -r + \alpha p + \frac{qS}{mV} C_{Y\beta} \beta$$

$$\dot{r} = \frac{I_{XZ}}{I_Z} \dot{p} + \frac{qSb^2}{2VI_Z} C_{n_r} r + \frac{qSb}{I_Z} C_{n\beta} \beta + \frac{qSb^2}{2VI_Z} C_{n\beta} \dot{\beta}$$

$$\dot{p} = \frac{qSb}{I_X} C_{l\beta} \beta$$

Taking the time derivative of the $\dot{\beta}$ equation assuming α is constant

$$\ddot{\beta} = -\dot{r} + \alpha \dot{p} + \frac{qS}{mV} C_{Y\beta} \dot{\beta}$$

Substituting and collecting terms gives

$$\ddot{\beta} - \left(\frac{qS}{mV} C_{Y\beta} - \frac{qSb^2}{2VI_Z} C_{n\beta} + \frac{qSb^2}{2VI_Z} C_{n_r} \right) \dot{\beta} + \left(\frac{qSb}{I_Z} C_{n\beta} - \frac{\alpha qSb}{I_X} C_{l\beta} + \frac{I_{XZ}qSb}{I_Z I_X} C_{l\beta} \right) \beta = 0$$

It is assumed that $r = -\dot{\beta}$ and the damping factor, ζ , is equal to

$$\frac{qS}{mV} C_{Y\beta} - \frac{qSb^2}{2VI_Z} C_{n\beta} + \frac{qSb^2}{2VI_Z} C_{n_r}$$

Therefore

$$\ddot{\beta} - \zeta \dot{\beta} + \left(\frac{qSb}{I_Z} C_{n\beta} - \alpha \frac{qSb}{I_X} C_{l\beta} + \frac{I_{XZ}qSb}{I_Z I_X} C_{l\beta} \right) \beta = 0$$

The natural frequency of the oscillation ω is determined from the imaginary part of the roots.

$$i\sqrt{\frac{\zeta^2 - 4\left(\frac{qSb}{I_Z} C_{n\beta} - \frac{\alpha qSb}{I_X} C_{l\beta} + \frac{I_{XZ}}{I_Z} \frac{qSb}{I_X} C_{l\beta}\right)}{2}} = \omega$$

Squaring and simplifying

$$C_{n\beta} = \frac{\omega^2 I_Z}{qSb} + \alpha \frac{I_Z}{I_X} C_{l\beta} - \frac{I_{XZ}}{I_X} C_{l\beta} + \frac{\zeta^2 I_Z}{4qSb}$$

Inasmuch as $\omega^2 = \left(\frac{2\pi}{P}\right)^2$ and $\zeta^2 = 4\left(\frac{0.693}{T_1/2}\right)^2$, substitution and rearrangement of terms gives

$$C_{n\beta} = \left[\left(\frac{2\pi}{P}\right)^2 + \left(\frac{0.693}{T_1/2}\right)^2 \right] \frac{I_Z}{qSb} + \alpha \frac{I_Z}{I_X} C_{l\beta} - \frac{I_{XZ}}{I_X} C_{l\beta}$$

where

$$C_{n_r} = \frac{\partial C_n}{\partial \frac{rb}{2V}}$$

$$C_{n_{\dot{\beta}}} = \frac{\partial C_n}{\partial \dot{\beta}}$$

$$C_Y = \frac{\text{Side force}}{qS}$$

$$C_{Y\beta} = \frac{\partial C_Y}{\partial \beta}$$

m mass

$$\dot{p} = \frac{\partial p}{\partial t}$$

$$\dot{r} = \frac{\partial r}{\partial t}$$

V velocity

$$\dot{\beta} = \frac{\partial \beta}{\partial t}$$

$$\ddot{\beta} = \frac{\partial^2 \beta}{\partial t^2}$$

REFERENCES

1. Williams, W. C., and Crossfield, A. S.: Handling Qualities of High-Speed Airplanes. NACA RM L52A08, 1952.
2. Ankenbruck, Herman O., and Dahlen, Theodore E.: Some Measurements of Flying Qualities of a Douglas D-558-II Research Airplane During Flights to Supersonic Speeds. NACA RM L53A06, 1953.
3. Ankenbruck, Herman O., and Wolowicz, Chester H.: Lateral Motions Encountered With the Douglas D-558-II All-Rocket Research Airplane During Exploratory Flights to a Mach Number of 2.0. NACA RM H54I27, 1954.
4. NACA High-Speed Flight Station: Flight Experience With Two High-Speed Airplanes Having Violent Lateral-Longitudinal Coupling in Aileron Rolls. NACA RM H55A13, 1955.
5. Bishop, Robert C., and Lomax, Harvard: A Simplified Method for Determining From Flight Data the Rate of Change of Yawing-Moment Coefficient With Sideslip. NACA TN 1076, 1946.

TABLE I

PHYSICAL CHARACTERISTICS OF AIRPLANE

Wing:

Airfoil section	NACA 64A007
Total area (including aileron and 83.84 sq ft covered by fuselage), sq ft	376.02
Span, ft	36.58
Mean aerodynamic chord, ft	11.33
Root chord, ft	15.86
Tip chord, ft	4.76
Taper ratio	0.30
Aspect ratio	3.56
Sweep at 0.25 chord line, deg	45
Incidence, deg	0
Dihedral, deg	0
Geometric twist, deg	0
Aileron:	
Area rearward of hinge line (each), sq ft	19.32
Span at hinge line (each), ft	7.81
Chord rearward of hinge line, percent wing chord	25
Travel (each), deg	±15
Irreversible hydraulic boost and artificial feel	
Aerodynamic balance	None
Static balance	Internal lead weights
Leading-edge slat:	
Span, equivalent, ft	12.71
Segments	5
Spanwise location, inboard end, percent wing semispan	24.6
Spanwise location, outboard end, percent wing semispan	94.1
Ratio of slat chord to wing chord (parallel to fuselage reference line), percent	20
Rotation, maximum, deg	15

Horizontal tail:

Airfoil section	NACA 65A003.5
Total area (including 31.65 sq ft covered by fuselage), sq ft	98.86
Span, ft	18.72
Mean aerodynamic chord, ft	5.83
Root chord, ft	8.14
Tip chord, ft	2.46
Taper ratio	0.30
Aspect ratio	3.54
Sweep at 0.25 chord line, deg	45
Dihedral, deg	0
Travel, leading edge up, deg	5
Travel, leading edge down, deg	25
Irreversible hydraulic boost and artificial feel	

TABLE I.- Concluded

PHYSICAL CHARACTERISTICS OF AIRPLANE

	A	B	C
Vertical tail:			
Airfoil section	NACA 65A003.5	NACA 65A003.5	NACA 65A003.5
Area (excluding dorsal fin and area blanketed by fuselage), sq ft	33.5	37.3	42.7
Area blanketed by fuselage (area between fuselage contour line and line parallel to fuselage reference line through intersections of leading edge of vertical tail and fuselage contour line)	2.11	2.11	2.45
Span (unblanketed), ft	6.14	7.45	7.93
Mean aerodynamic chord, ft	5.83	5.51	5.90
Root chord, ft	7.75	7.75	8.28
Tip chord, ft	3.32	2.32	2.49
Taper ratio	0.428	0.301	0.301
Aspect ratio	1.13	1.49	1.49
Sweep at 0.25 chord line, deg	45	45	45
Rudder:			
Area, rearward of hinge line, sq ft	6.3	6.3	6.3
Span at hinge line, ft	3.33	3.33	3.33
Root chord, ft	2.27	2.27	2.27
Tip chord, ft	1.50	1.50	1.50
Travel, deg	±20	±20	±20
Spanwise location, inboard end, percent vertical tail span	4.5	3.7	3.1
Spanwise location, outboard end, percent vertical tail span	58.2	48.0	44.8
Chord, percent vertical tail chord	30.0	30.0	28.4
Aerodynamic balance	Overhanging, unsealed	Overhanging, unsealed	Overhanging, unsealed
Fuselage:			
Length (afterburner nozzle closed), ft			45.64
Maximum width, ft			5.58
Maximum depth over canopy, ft			6.37
Side area (total), sq ft			230.92
Fineness ratio (afterburner nozzle closed)			7.86
Speed brake:			
Surface area, sq ft			14.14
Maximum deflection, deg			30
Power plant:			
Turbojet engine	One Pratt & Whitney J57-P7 with afterburner		
Thrust (guarantee sea level), afterburner, lb			15,000
Military, lb			9,220
Normal, lb			8,000
Airplane weight, lb:			
Basic (without fuel, oil, water, pilot)			19,662
Total (full fuel, oil, water, pilot)			24,800
Center-of-gravity location, percent \bar{x}:			
Total weight - gear down			31.80
Total weight - gear up			31.80
Moments of inertia (estimated total weight):			
I_x , slug-ft ²			11,103
I_y , slug-ft ²			59,248
I_z , slug-ft ²			67,279
I_{xz} , slug-ft ²			941
Inclination of principal axis (estimated total weight):			
B.C.C. reference axis at nose, deg			0.8

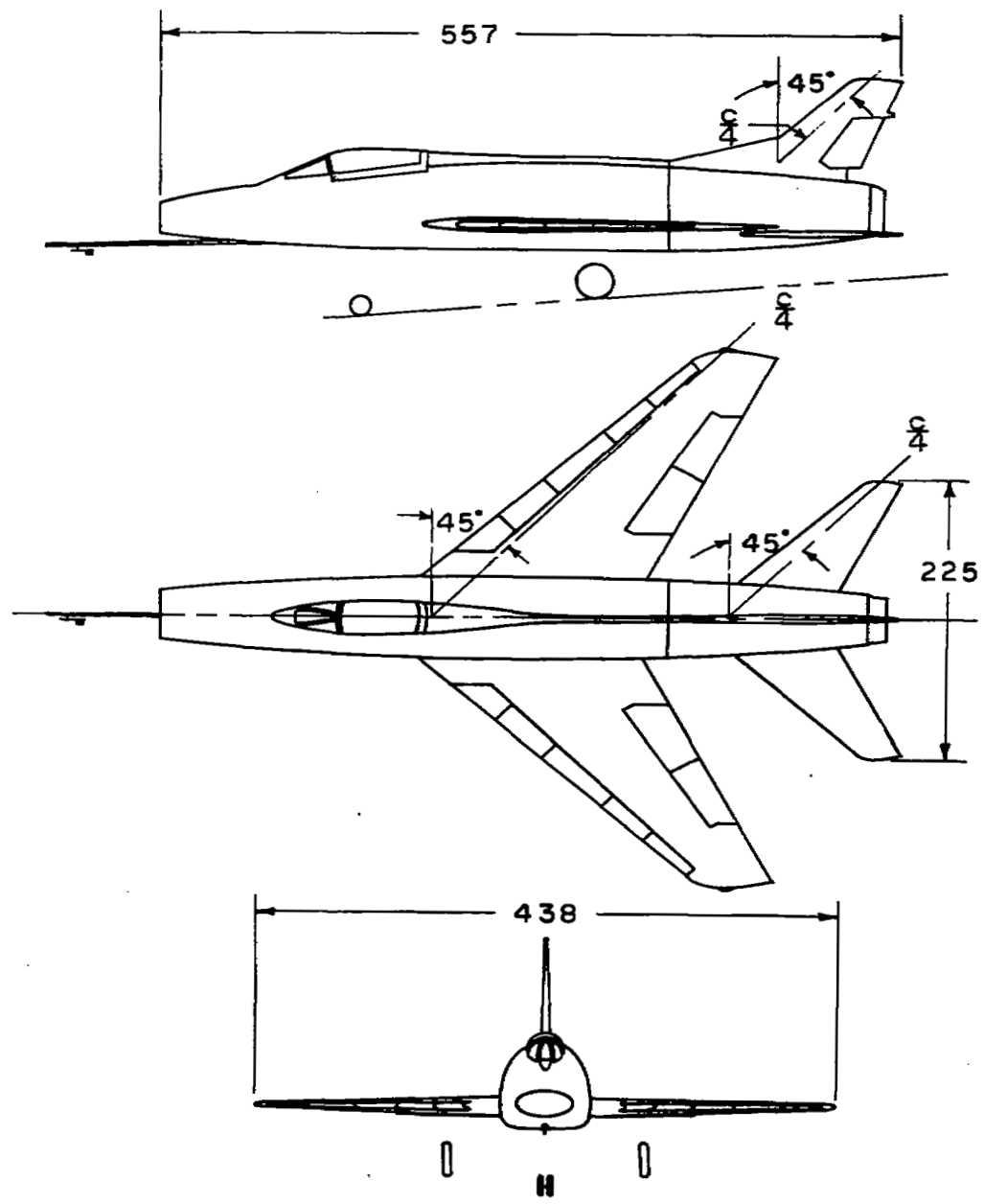


Figure 1.- Three-view drawing of airplane with vertical tail A. All dimensions in inches.

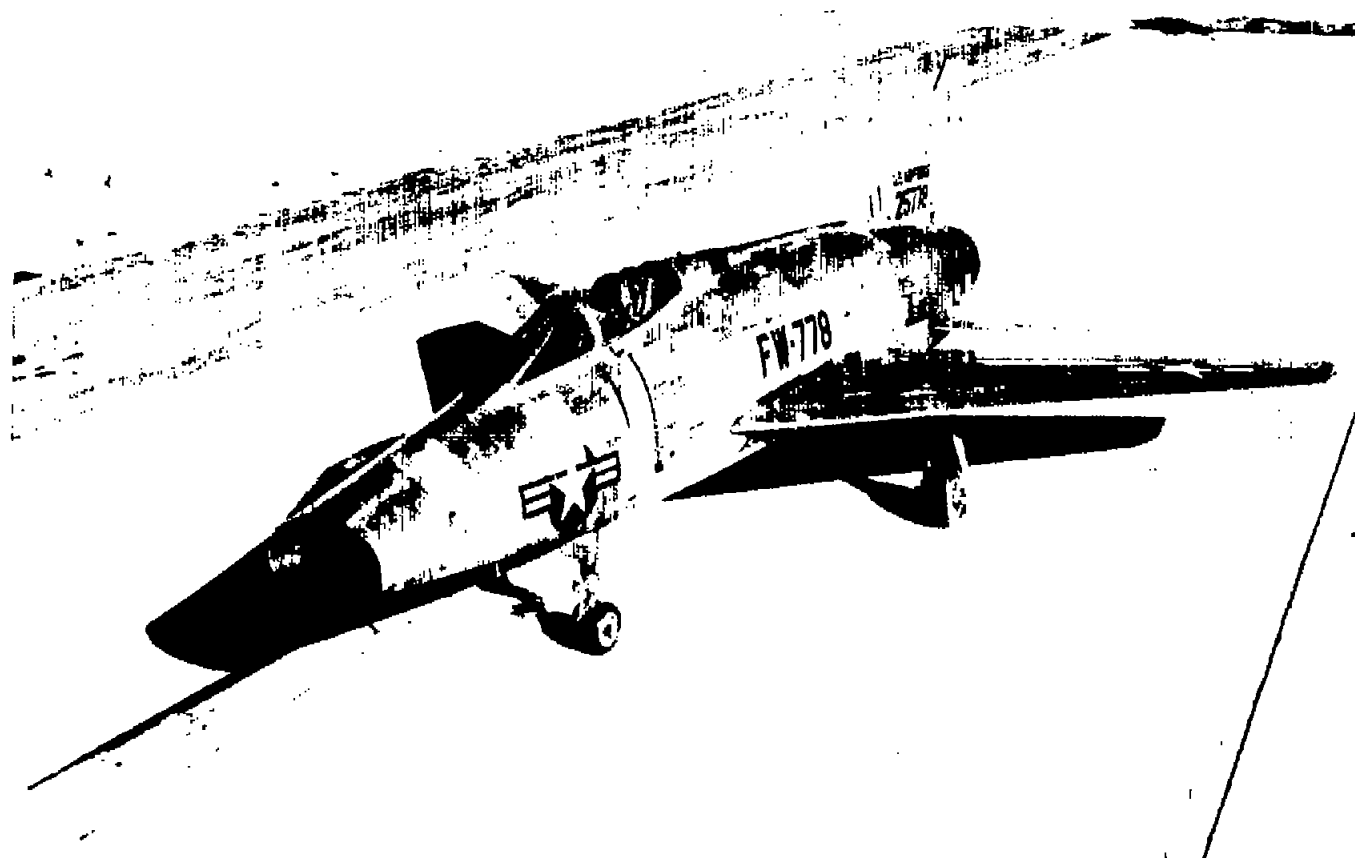
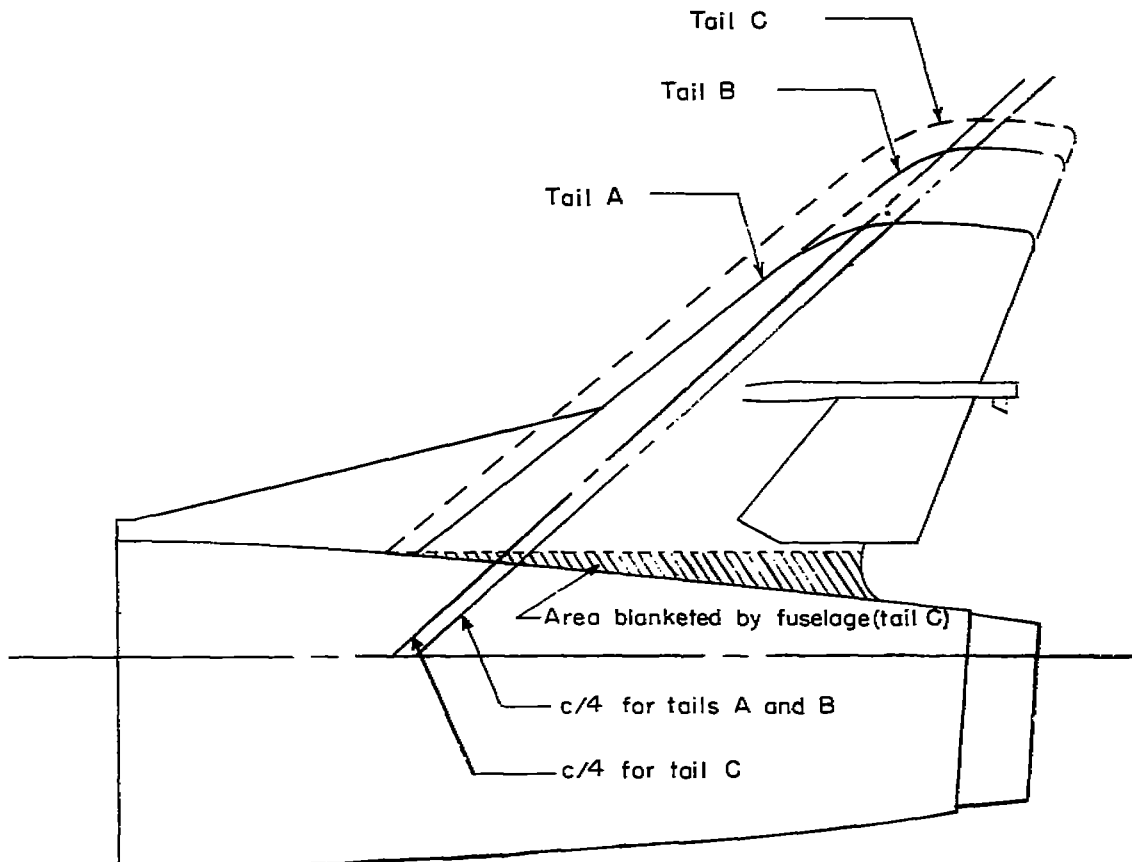


Figure 2.- Photograph of the airplane.

L-89375



Tail	$\Lambda_c/4$, deg	A	λ	Area, sq ft (1)	Span, ft (2)	Blanketed area, sq ft
A	45°	1.13	0.428	33.5	6.14	2.11
B	45°	1.49	0.301	37.3	7.45	2.11
C	45°	1.49	0.301	42.7	7.93	2.45

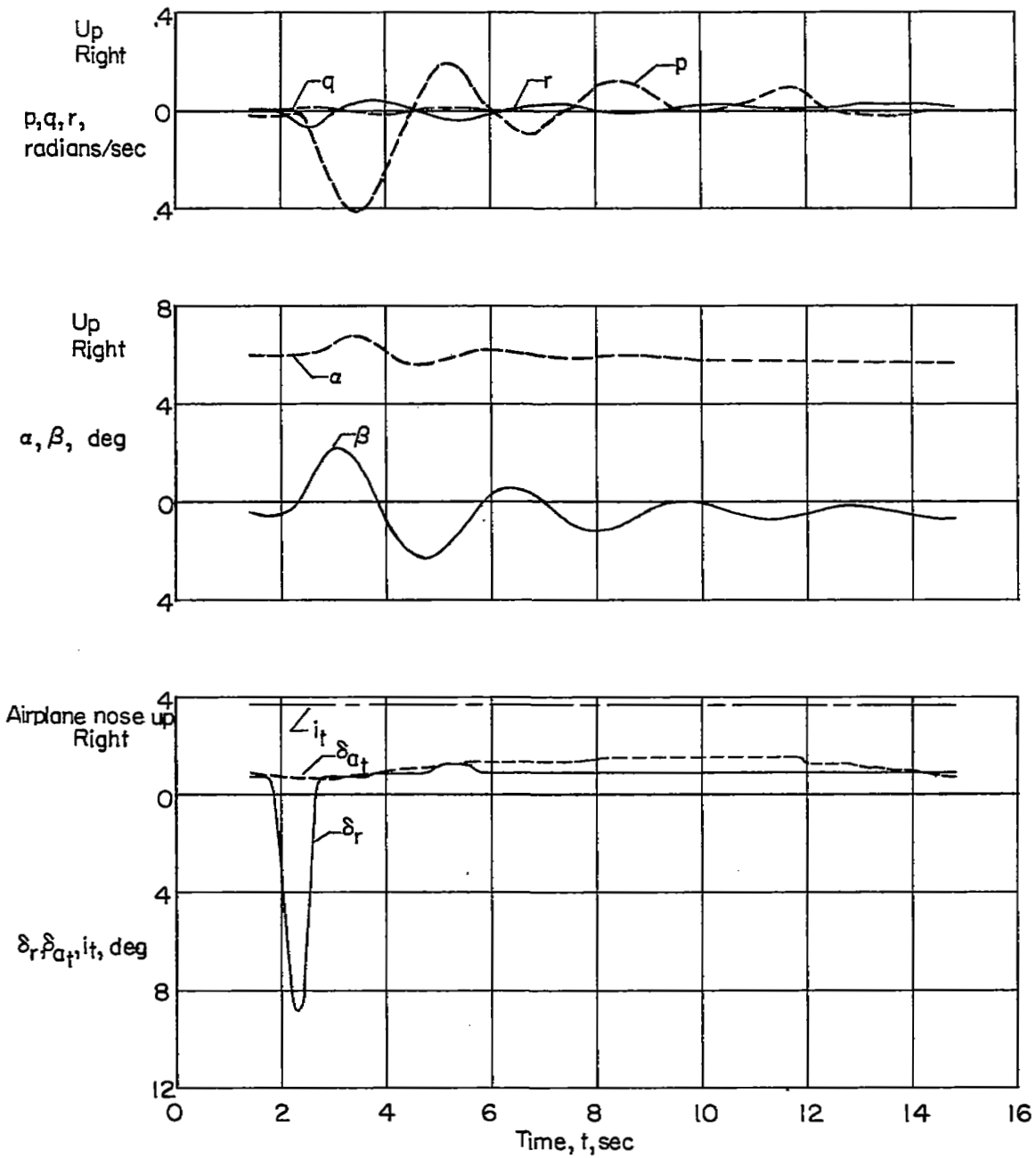
(1) Area not blanketed by fuselage

(2) Span not blanketed by fuselage

Figure 3.- Sketch of vertical tails A, B, and C.

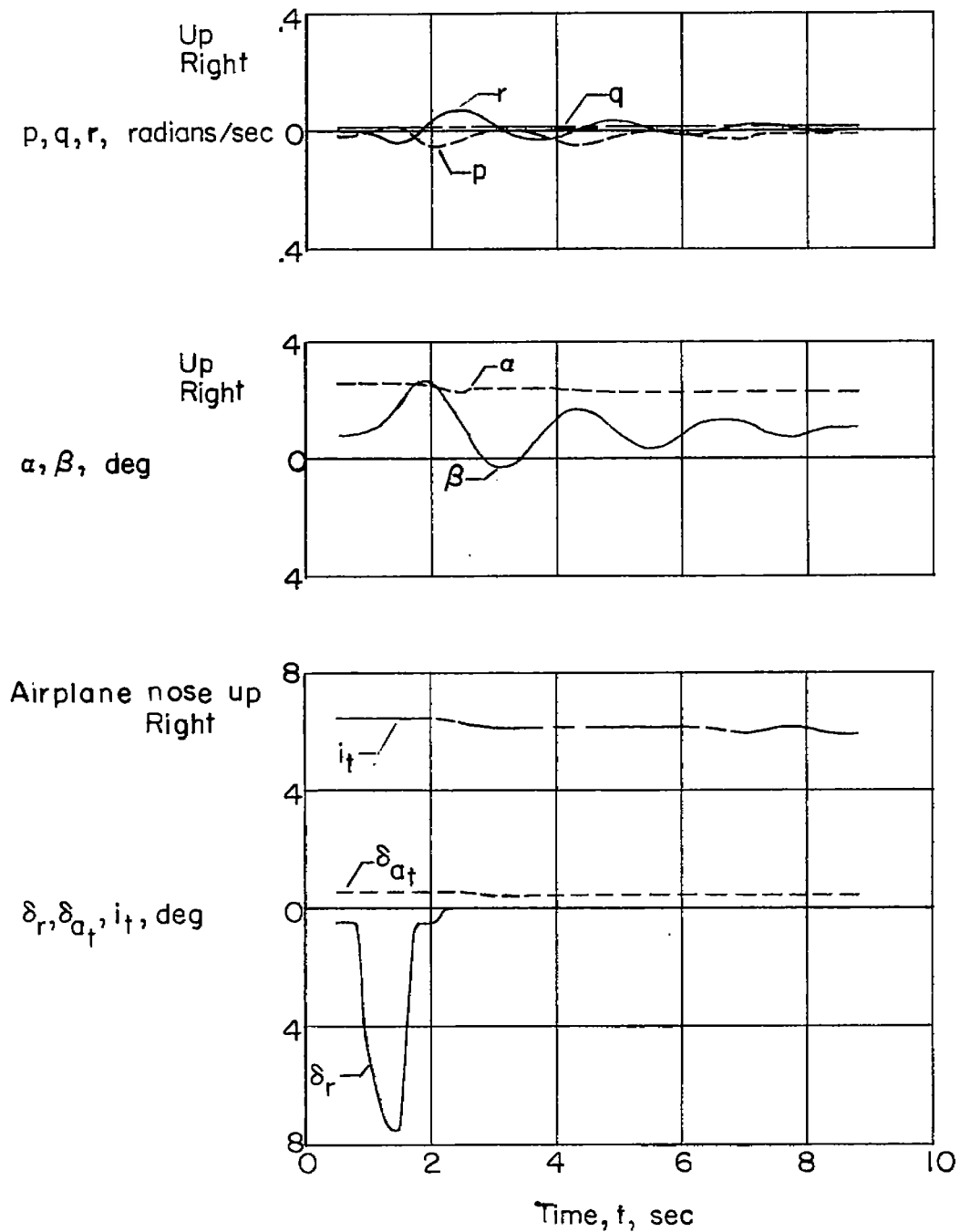


Figure 4.- Photograph of two airplanes showing tails A and C. L-89376



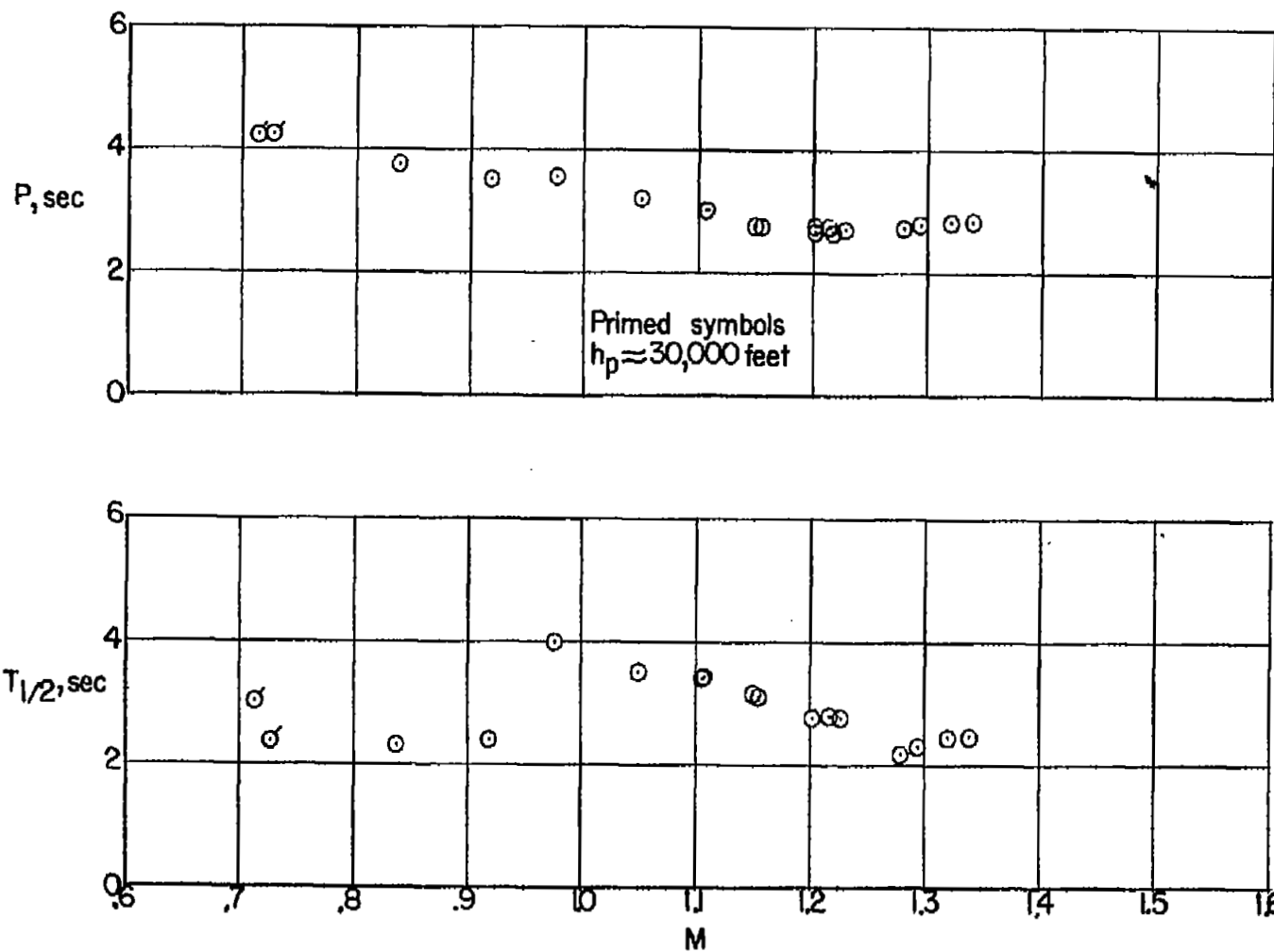
(a) $M \approx 0.74$; $h_p \approx 30,000$ feet.

Figure 5.- Time history of lateral oscillation induced by a rudder pulse for airplane with vertical tail (B).



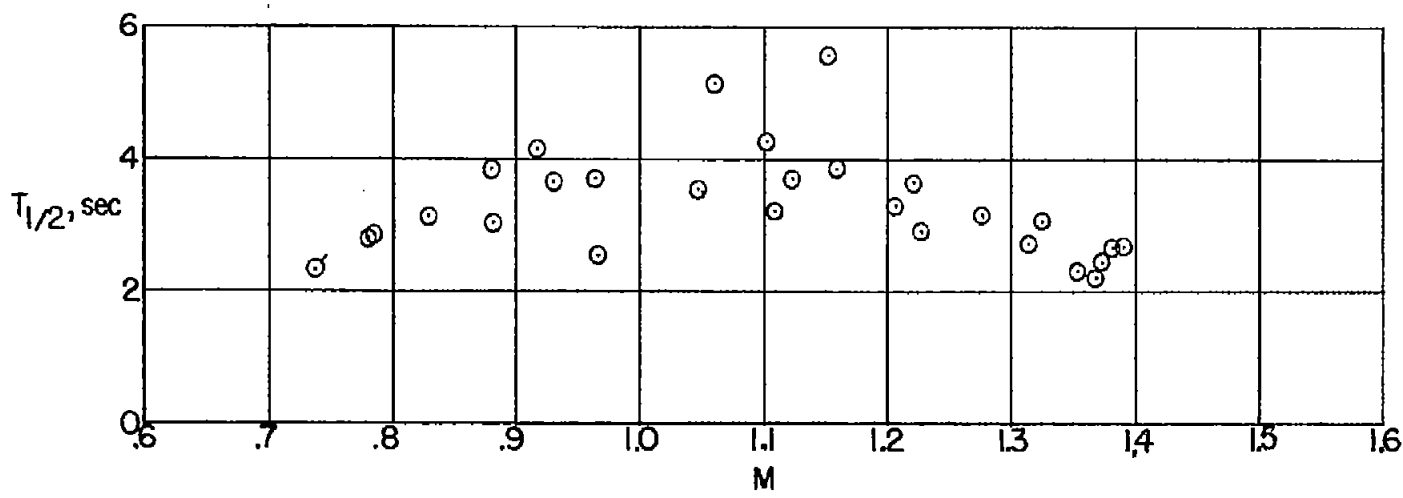
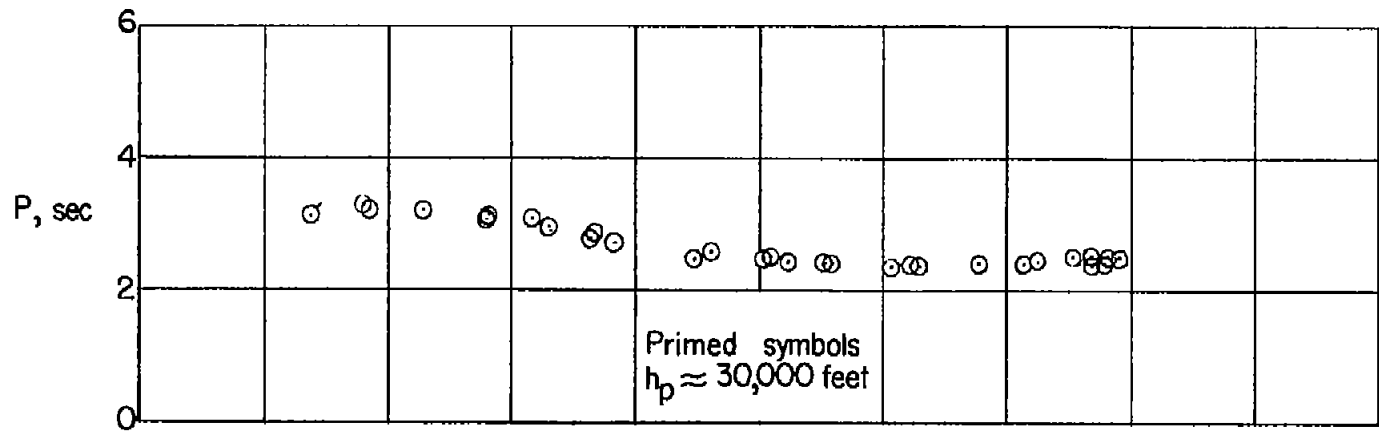
(b) $M \approx 1.38$; $h_p \approx 37,000$ feet.

Figure 5.- Concluded.



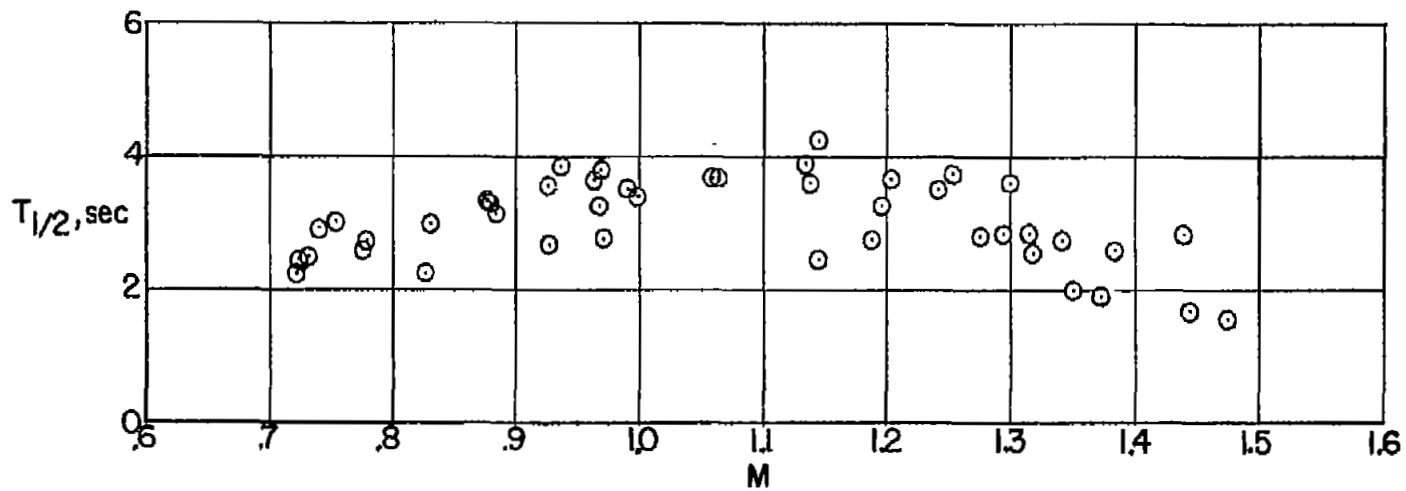
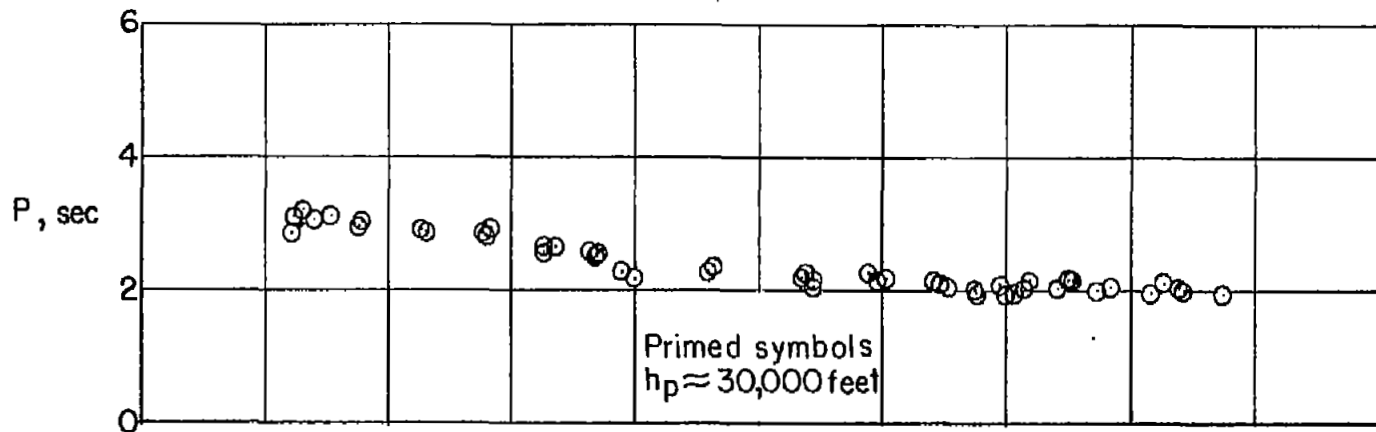
(a) Vertical tail A.

Figure 6.- Mach number variation of period and time to damp to half-amplitude of lateral oscillation for altitudes near 40,000 feet.



(b) Vertical tail B.

Figure 6.- Continued.



(c) Vertical tail C.

Figure 6.- Concluded.

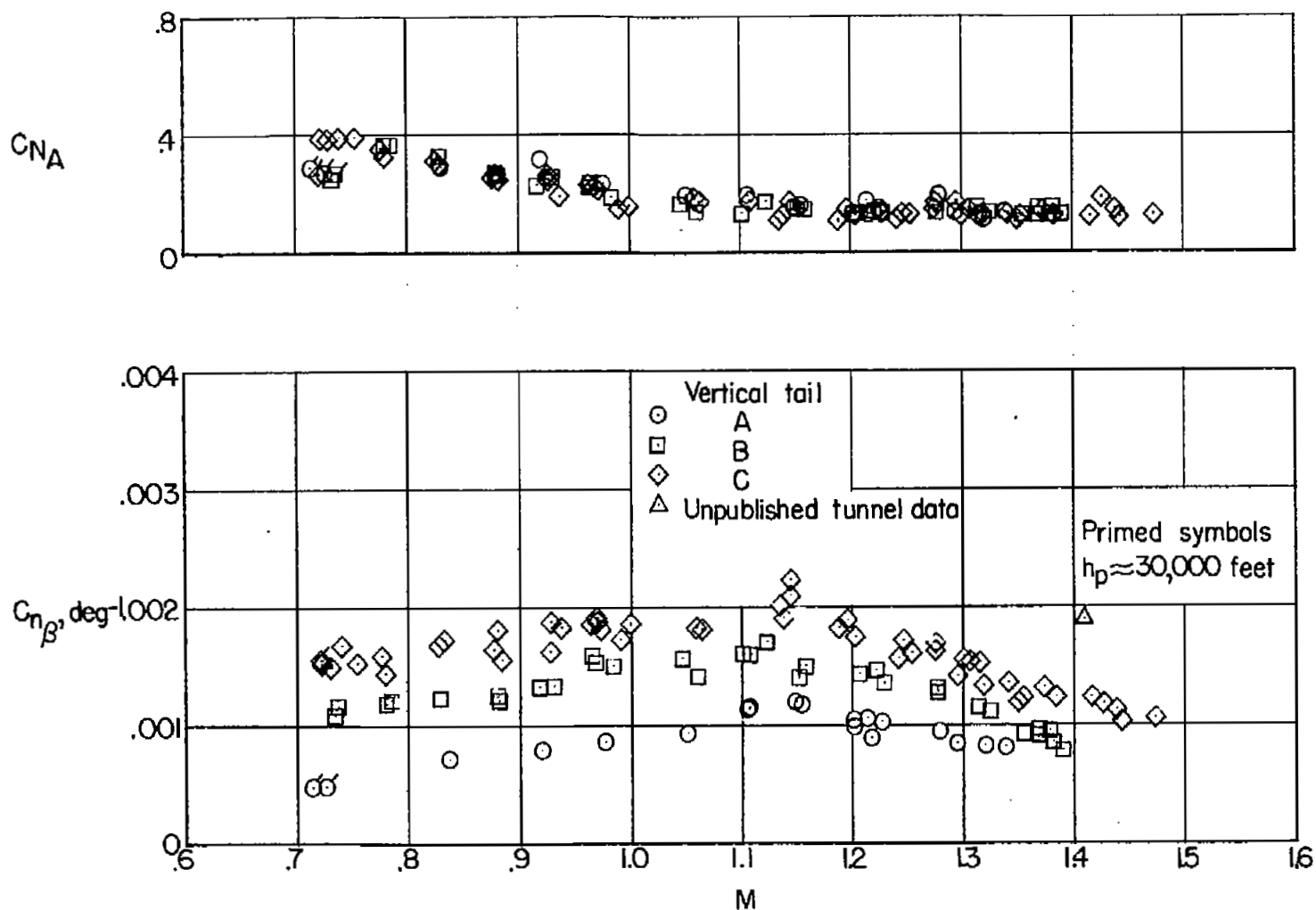


Figure 7.- Mach number variation of directional stability parameter $C_{n\beta}$ for three vertical tail configurations at altitudes near 40,000 feet.

